

Adsorption-induced strain of a nanoscale silicon honeycomb

A. GROSMAN¹, J. PUIBASSET² and E. ROLLEY³

¹ *Institut des NanoSciences de Paris, CNRS, UPMC Univ. Paris 6 - 4, place Jussieu, 75005 Paris, France*

² *Interfaces, Confinement, Matériaux et Nanostructures, CNRS UMR7374, Université d'Orléans
1b rue de la Férollerie, 45071 Orléans cedex 02, France*

³ *Laboratoire de Physique Statistique de l'ENS, associé au CNRS et aux Universités Paris 6 et Paris 7
24 rue Lhomond, 75005 Paris, France*

received 5 December 2014; accepted in final form 25 February 2015
published online 13 March 2015

PACS 68.43.-h – Chemisorption/physisorption: adsorbates on surfaces

PACS 62.20.de – Elastic moduli

Abstract – We report on systematic measurements of both adsorption and anisotropic mechanical deformations of mesoporous silicon, using heptane at room temperature. Porous Si obtained from highly doped (100) Si can be thought of as a nanoscale random honeycomb with pores parallel to the [001] axis. We show that strains ϵ_{\parallel} and ϵ_{\perp} measured along and transversely to the pore axis exhibit a hysteretic behavior as a function of the fluid pressure, which is due to the hysteresis in fluid adsorption. The pressure dependence of the strains together with the independent measurement of the transverse stress, allows us to determine the biaxial transverse modulus and to estimate the longitudinal Young's modulus of porous Si. We argue that the value of these constants implies that Young's modulus of the 6 nm thick walls of the honeycomb is about 5 times smaller than that of bulk silicon, striking evidence of finite-size effects.

Copyright © EPLA, 2015

Introduction. – Porous silicon (PoSi) has been extensively studied, originally for its optical and electrical properties and more recently for its mechanical properties. A large variety of pore morphologies and a large range of porosities can be obtained depending on the doping and etching conditions [1]. In this paper, we focus on PoSi obtained from highly p-doped (100) Si wafers. In this case, etching leads to straight pores aligned with the [001] axis [2]. For about 10 years, this system has received renewed attention as a model system for adsorption studies [3]. One of the intriguing features of this system is that the emptying of liquid-filled pores occurs in a collective-like process. This is usually attributed to the connectivity of the pore network [4] but pores in PoSi are non-connected [3]. Thus, the apparent collective behavior has been attributed to disorder inside each pore [5] or to the adsorption-induced mechanical deformation of the pore walls [6].

In order to test this idea, the first step is to check whether such a material as stiff as porous single crystal Si can be deformed by capillary forces. A first attempt by Dolino *et al.* [7] has shown the existence of such a deformation, but no systematic and precise comparison between the strain and the amount of adsorbed fluid was performed. More recently, other porous systems have

been studied [8–10] and theoretical models and simulations developed [11–13].

The second goal of the present work is to get a better understanding of the elastic properties of PoSi. Recently, several groups measured the elastic modulus through nano-indentation experiments [14,15]. However, such a technique can yield the value of Young's modulus only if the material is isotropic and if Poisson's ratio is hypothesized. Though nano-indentation results are roughly consistent with PoSi being described as a 3D isotropic foam, they do not provide strong evidence for it. While the structure of *some* PoSi samples is indeed close to an isotropic foam, this is not the case for the system we are investigating. Acoustic wave propagation [16] and Brillouin [17] scattering have also been used for the determination of elastic constants of PoSi. Most of these experiments have been analyzed taking into account the underlying cubic symmetry of the Si lattice but neglecting the important anisotropy of the aligned straight pores.

In this paper, we report on systematic measurements of adsorption-induced strain in mesoporous Si which is a realization of a disordered honeycomb at the unusual nanometer scale (fig. 1). In the next section, we describe the experimental techniques, mainly the novel optical apparatus used to measure the strains ϵ_{\parallel} and ϵ_{\perp} along

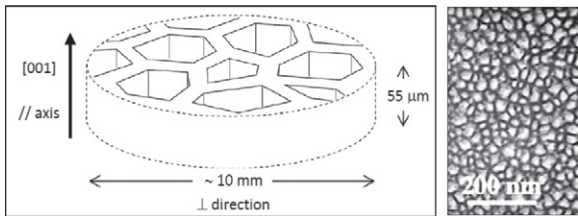


Fig. 1: Schematic view of the sample geometry and transmission electron microscopy plane view of a 70% porosity sample.

and transversely to the pore axis, during an adsorption-desorption cycle as a function of the gas pressure P . In the third section, we discuss qualitatively the shape of the hysteresis cycles of the strains and amount adsorbed. The fourth section is devoted to a numerical study of the elastic deformation induced by a confined fluid at the nanoscale. We validate the sharp interface approximation used to analyze quantitatively the experimental data. The fifth section is devoted to a quantitative discussion of the reversible branch of the cycle when pores are full of liquid. In this situation, the liquid in the core of pores is at negative pressure, P_L . We have measured the effective moduli $M_{\parallel,\perp} \equiv dP_L/d\epsilon_{\parallel,\perp}$ which can be related to elastic moduli of the porous material. Finally, we show that the values of these moduli and their dependence on the porosity are consistent with a honeycomb structure whose silicon walls have a Young's modulus several times smaller than that of bulk silicon.

Samples and setups. – *Samples:* Details about sample preparation and full characterization have been published elsewhere [2]. The samples have nominal porosity p of 50% and 70%, obtained by etching (100) Si wafers. The pores are straight, non-connected and perpendicular to the wafer surface. The pore cross-section is roughly polygonal in shape and the pore radius distribution is large, 6.5 ± 3 nm and 13 ± 7 nm for 50% and 70% porosity. Thus, the porous layer can be thought of as a random nanoscale honeycomb. The thickness of the wall between pores is 5–6 nm, independently of the porosity. The thickness of the porous layers used in the present work is $55 \mu\text{m}$. These porous layers were studied both attached to the underlying Si wafer (supported layers) or detached from the wafer (membranes).

Adsorption isotherms: The adsorbed amount of n -heptane is measured at $T = 18^\circ\text{C}$ as a function of the increasing and decreasing gas pressure P with a commercial apparatus (Micromeritics ASAP2010).

Transverse strain of membranes: Two sample pieces (of cm size) are mounted opposite to each other, with a small gap left between their free ends. The gap decreases upon porous samples expansion. The gap is measured with a CCD camera equipped with a high-magnification objective. The advantage of this symmetric geometry is to cancel the effect of a possible drift of the camera with respect to the cell: a drift changes the gap position on

the CCD but not its width. The final uncertainty on ϵ_{\perp} is 10^{-7} . The samples were cut randomly with respect to the crystal axis without measurable effect on ϵ_{\perp} . Thus, we will neglect any anisotropy transverse to the pore direction.

Longitudinal strain of membranes: The order of magnitude of ϵ_{\parallel} is the same as that of ϵ_{\perp} but the deformation along the pore axis is much smaller since the membranes are only a few tens of micrometers thick. Thus, a different setup was used: a small piece of membrane is sandwiched between a mirror and a semi-reflecting plate. The sample is free to expand in transverse direction. In both setups, the samples are held in place with soft springs so that the external stress is negligible compared to the sorption stress. The two optical components form a wedge whose small angle depends on the membrane thickness. When illuminated with a He-Ne laser, one obtains equal thickness fringes which shift when the sample thickness changes. The amplitude of the deformation being of the order of 10 nm, the fringe shift is small, of the order of a tenth of a fringe. This means that phase change induced by the change in gas pressure has to be corrected. To this end, we measured the optical index of n -heptane prior to the adsorption experiment. In the end, the accuracy is limited by thermal drift of the whole setup, including the CCD camera. The final uncertainty on ϵ_{\parallel} is about 10^{-6} , an order of magnitude larger than for ϵ_{\perp} .

In contrast to adsorption isotherms which are measured for discrete values of the gas pressure P , strains $\epsilon_{\parallel}(P)$ and $\epsilon_{\perp}(P)$ are scanned by changing continuously the pressure at a constant rate. The usual duration of a whole cycle is 6 hours. Whatever the duration between 4 to 12 hours, the cycle remains unchanged, except for the emptying which appears smoother at high sweeping rate.

Qualitative behavior. – Both the adsorption isotherm and strains are shown in fig. 2 for a 50% porosity membrane. The shape of the isotherm is similar to that obtained with a simple fluid such as nitrogen or argon. Condensation in pores happens progressively up to 25 mbar while evaporation occurs rather abruptly around 15 mbar. For a 70% porosity membrane, the isotherm is similar, the pressures being shifted to higher values.

The variations of the strains during a cycle also display an hysteresis (fig. 2). At low pressure, on the reversible part A of the isotherm, the film adsorption is accompanied by an extension along the pore axis and a clear contraction along the transverse direction up to a few mbars. This transverse contraction is remarkable: in isotropic materials such as porous glass [10,18] or carbon [9] a marked expansion is always observed. In the case of porous silica SBA-15 [8] and MCM-41 [11] expansion transverse to the pore axis is also observed (ϵ_{\parallel} has not been measured in these systems). On branch B, the pores fill progressively from the smallest to the largest, creating concave menisci at the pore ends. The liquid is then at negative pressure so that both ϵ_{\parallel} and ϵ_{\perp} start decreasing. When all the pores

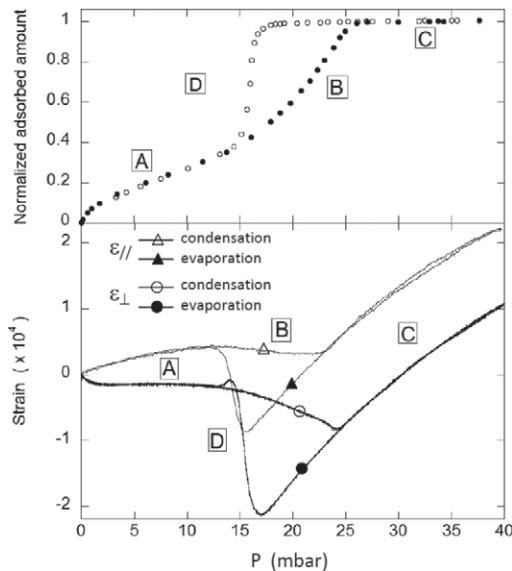


Fig. 2: Upper graph: adsorption of *n*-heptane at 18 °C in a 50% porosity membrane (saturated vapor pressure $P_0 = 42.5$ mbar). Lower graph: parallel and transverse strains $\epsilon_{||}$ and ϵ_{\perp} .

are full of liquid, on the saturation plateau (branch C), the liquid pressure increases with the gas pressure: the material expands.

Decreasing P from the saturated vapor pressure P_0 , the material contracts reversibly on the saturation plateau until evaporation starts (D). When all the pores are empty, one recovers the reversible film branch A. As noted earlier, the emptying branch D is difficult to measure. Since evaporation occurs in a narrow pressure range, the position and shape of the D branch is dependent on the pressure rate dP/dt , even at the lowest rate when evaporation takes place in about one hour. This is especially true for $\epsilon_{||}$: in the interferometric setup, the membrane is sandwiched between two optical surfaces and the “open ends” of the pores are partially obstructed. The ϵ_{\perp} measurement is not very accurate in the D branch for another reason: the emptying of the pores triggers a slight curvature of the sample, which, in turn, causes a slight defocusing of the free edge of the sample and a small change in the reflected intensity. This is the reason why a small overshoot can be seen at the end of the branch D. This overshoot is due to an optical artifact sensitive to the optical alignment. However, the branch D is the only one which is difficult to determine. In particular, the two reversible branches are straightforward to measure with a good accuracy, as shown by the overlap of the adsorption and desorption curves.

Similar strain cycles are observed for 70% porosity samples, but shifted to higher pressure by the same amount as the adsorption cycle.

In conclusion, the shape of $\epsilon_{||}(P)$ is roughly similar to the strain in other mesoporous materials. The main qualitative difference of PoSi is the contraction of $\epsilon_{\perp}(P)$ at low pressure. A phenomenological model recently developed

by Neimark and co-workers has been able to explain the observed behavior in porous silica [12,19], which consists in a regular array of parallel cylindrical pores. Though this model provides a useful theoretical framework, its present implementation is not relevant for our system. First, the model does not consider any strain along the pore axis while we find that both strains are of the same order. Second, the model cannot explain the transverse contraction at low pressure. The origin for this contraction is a completely open question.

Molecular simulations. – As shown by Günther *et al.* [11], a simple molecular model including dispersion forces is able to catch the main physics of sorption-induced deformations. We use the standard grand canonical Monte Carlo algorithm to mimic the experimental situation where the chemical potential of the adsorbed fluid is imposed through the pressure P of the surrounding gas. The details of the cross-sectional geometry of PoSi are discarded, the important point being the strong anisotropy. The pore model is thus chosen to be an infinite cylinder (periodic boundary conditions are applied along the pore axis). *n*-heptane being a non-polar fluid, the fluid-fluid and fluid-pore interactions are van der Waals and can be described by the Lennard-Jones (LJ) potential $4\epsilon[(\sigma/r)^{12} - (\sigma/r)^6]$. For this preliminary study, we make the assumption that the molecules are spherical. Following Watanabe *et al.* [20], the potential is truncated at 3σ and a quadratic term is added so that both the potential and force are continuous. The fluid-fluid parameters $\sigma_{ff} = 0.6$ nm and $\epsilon_{ff}/k = 505$ K, where k is Boltzmann’s constant, allow us to reproduce the experimental *n*-heptane phase diagram, except for its freezing point, probably because *n*-heptane is actually made of linear chains. In order to remain in the liquid phase, calculations are thus performed at 353 K, just above the LJ freezing point.

For the fluid-wall parameters we chose $\sigma_{fw} = \sigma_{ff}$, and ϵ_{fw} so that the adsorption-desorption hysteresis is between $P/P_0 = 0.4$ and 0.8 for the range of pore radii studied (see fig. 3). The pore radii are given by the position of the Gibbs surface defined so that the excess amount adsorbed is zero: the saturation branches then superimpose to the bulk data.

The relevant thermodynamic potential is the grand potential $\Omega(\mu, V, T)$, where μ is the chemical potential, V the volume and T the temperature. For fixed T and μ , $d\Omega = -P_{th}dV$, where P_{th} is the so-called thermodynamic pressure. For bulk fluid, P_{th} is identical to the mechanical pressure. For a liquid confined in a cylindrical pore, the sharp interface approximation gives: $\Omega = -\pi r_p^2 l P_L + 2\pi r_p l \gamma$ so that $P_{th} = P_L - 2\gamma/r_p$, where r_p and l are the pore radius and length, and γ the fluid-wall surface tension. P_{th} is the relevant quantity to be considered when the pore deforms along its axis. Note that this pressure differs from the solvation pressure defined in ref. [12], where only transverse strain is considered.

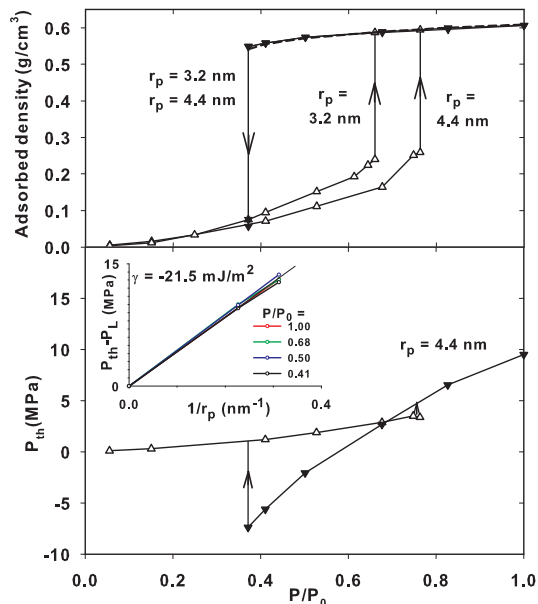


Fig. 3: (Colour on-line) Adsorption isotherms and thermodynamic pressure P_{th} for a Lennard-Jones fluid confined in cylindrical pores. Lines are a guide to the eye. Dashed line in the upper panel: bulk liquid, indistinguishable from the saturation branches. Inset: $P_{\text{th}} - P_L$ vs. $1/r_p$ for various P/P_0 .

P_{th} has been calculated during the course of the simulation [21–23] (see fig. 3, lower panel). Upon adsorption (open symbols), the fluid is confined close to the pore wall, resulting in a positive spreading pressure in the directions parallel to the wall, in particular along the pore axis. When the pore is filled with liquid, an extra negative contribution comes from the liquid under tension for $P/P_0 < 1$. The relation $P_{\text{th}} = P_L - 2\gamma/r_p$ is well verified for the pore studied with $\gamma = -21.5 \text{ mJ/m}^2$ (inset in fig. 3). The sharp interface approximation is thus valid for $r_p \geq 3.2 \text{ nm}$, corresponding to the experimental samples.

We now focus on a deformable pore. To keep the model simple, we suppose that the pore deforms along its axis only. The elastic modulus of walls has been chosen as low as 1 GPa in order to enhance deformations and possible effects on the adsorption isotherms. As a matter of fact, no effect has been observed on the isotherms (less than 5×10^{-4} relative difference). Still, a deformation is observed along the condensation-evaporation curves. We find that the strain ϵ_{\parallel} is proportional to P_{th} and that the ratio $P_{\text{th}}/\epsilon_{\parallel}$ is consistent with the elastic modulus of the pore wall. Note that this is true whatever the modulus value (within the 5% uncertainty of the numerical data), showing that the system is in the linear elastic regime. These results have two important consequences: i) the variation of P_{th} as a function of P/P_0 should be qualitatively similar to the measured $\epsilon_{\parallel}(P)$, and this is indeed the case; ii) the pore sizes in our samples are large enough for the strain dependence with P_{th} to be equal to the dependence with P_L , the parameter which can be obtained experimentally.

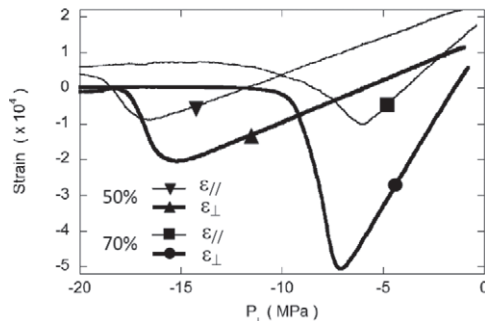


Fig. 4: Strains as a function of the liquid pressure P_L . Only data corresponding to a decreasing gas pressure are shown.

Table 1: Measured elastic responses to inner pressure P_L .

Sample	Porosity p	M_{\parallel} (GPa)	M_{\perp} (GPa)	$\frac{d\sigma_{\perp}}{dP_L}$	$\frac{dP_L}{d\epsilon'_{\perp}}$ (GPa)
50%	0.512	47	42.5	0.38	320
70%	0.704	18.1	10.6	0.57	270

Elastic constants of porous silicon. – In fig. 4, the strains ϵ_{\parallel} and ϵ_{\perp} are plotted as a function of the equilibrium liquid pressure $P_L = RT/V_L \ln(P/P_0)$, where R is the ideal gas constant and V_L , the molar volume of the liquid. As expected, we find that the strains are perfectly linear in P_L along the saturation plateau. This allows us to define the effective elastic moduli $M_{\parallel, \perp} \equiv \frac{dP_L}{d\epsilon_{\parallel, \perp}}$ which characterize the response of the porous material when submitted to an homogeneous inner pressure. The values for M_{\parallel} and M_{\perp} are summarized in table 1.

Another independent elastic modulus can be obtained using supported layers, as suggested by Barla *et al.* [24]. If the porous material is still attached to the wafer, adsorption process induces a stress in the porous layer which results in a bending of the structure. The radius of curvature R is easily measured with standard optical interferometry. The variation of $1/R$ with P is shown in fig. 5 for a supported layer of 50% porosity.

For our samples, the thickness ($d_P = 55 \mu\text{m}$) and modulus (as shown below) of the porous layer are much smaller than those of underlying bulk Si ($d_S = 220 \mu\text{m}$). In this case, the neutral surface is very close to the middle of the bulk layer and the average strain ϵ'_{\perp} of the porous layer varies with the curvature $1/R$ as: $d\epsilon'_{\perp}/d(1/R) = (d_S + d_P)/2$. Following Reinhart and Logan [25], the transverse stress σ_{\perp} exerted on the porous layer by the underlying bulk layer reads

$$\sigma_{\perp} = -\frac{1}{R} \frac{1}{6d_P(d_S + d_P)} \left(\frac{d_S^3}{S_S} + \frac{d_P^3}{S_P} \right). \quad (1)$$

S_S and S_P are the compliances of the bulk and PoSi: $S_S = (1 - \nu)/E = 1/180 \text{ GPa}^{-1}$ ($E = 130 \text{ GPa}$ and $\nu = 0.28$ for (100) wafers [26]). In the worst case, the correction due

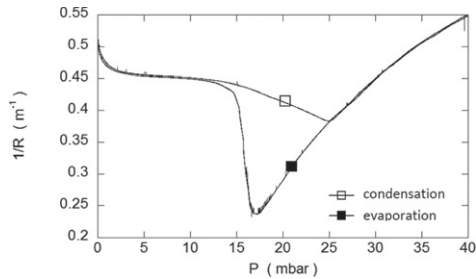


Fig. 5: Inverse radius of curvature as a function of the gas pressure P for a 50% porosity supported layer. Note the similarity with $\epsilon_{\perp}(P)$ in fig. 2.

to the second term in σ_{\perp} is 3% and will be neglected. We find that σ_{\perp} varies linearly with P_L . Values for $\frac{d\sigma_{\perp}}{dP_L}$ and $\frac{dP_L}{de_{\perp}}$ are given in table 1.

The next step is to relate the 3 response coefficients M_{\parallel} , M_{\perp} and $\frac{d\sigma_{\perp}}{dP_L}$ to the “fundamental” elasticity quantities of Young’s modulus (E) and Poisson’s ratio (ν). Choosing [100], [010] and [001] as the axes ([001] is the pore axis), the compliance matrix can be written as

$$\begin{pmatrix} \epsilon_1 \\ \epsilon_2 \\ \epsilon_3 \end{pmatrix} = \begin{pmatrix} \frac{1}{E_1} & -\frac{\nu_{12}}{E_1} & -\frac{\nu_{31}}{E_3} \\ -\frac{\nu_{12}}{E_1} & \frac{1}{E_1} & -\frac{\nu_{31}}{E_3} \\ -\frac{\nu_{13}}{E_1} & -\frac{\nu_{13}}{E_1} & \frac{1}{E_3} \end{pmatrix} \begin{pmatrix} \sigma_1 \\ \sigma_2 \\ \sigma_3 \end{pmatrix} \quad (2)$$

with $\frac{\nu_{13}}{E_1} = \frac{\nu_{31}}{E_3}$. We have used the fact that axes (1) and (2) ([100] and [010], respectively) are equivalent and we have not written the shear components since there is no shear stress in our experiments. We are left with 4 unknown elastic coefficients while i) we have measured only 3 independent quantities, ii) we still have to relate the liquid pressure P_L in the pore to the average stresses $\sigma_{1,2,3}^i$ (superscript i stands for stresses originating from inner pore pressure). For the pore direction (3), the balance of forces gives $\sigma_3^i = pP_L$, where p is the porosity. However, there is no simple way to obtain the two in-plane components $\sigma_{1,2}^i(P_L)$ which are equal in our experiments: $\sigma_{1,2}^i(P_L) \equiv \sigma_{\perp}^i(P_L)$. For free membranes, we thus have

$$\epsilon_{\perp} = \frac{1 - \nu_{12}}{E_1} \sigma_{\perp}^i(P_L) - \frac{\nu_{13}}{E_1} pP_L, \quad (3)$$

$$\epsilon_{\parallel} = -\frac{2\nu_{31}}{E_3} \sigma_{\perp}^i(P_L) + \frac{1}{E_3} pP_L. \quad (4)$$

And for supported layers:

$$\epsilon'_{\perp} = \frac{1 - \nu_{12}}{E_1} [\sigma_{\perp}(P_L) + \sigma_{\perp}^i(P_L)] - \frac{\nu_{13}}{E_1} pP_L. \quad (5)$$

The numerical values in table 1 allow to calculate the biaxial modulus $E'_1 \equiv \frac{E_1}{1 - \nu_{12}}$. One finds 18.6 and 6.2 GPa for the 50% and 70% porosity samples. One can also compute E_3 as a function of ν_{31} . For ν_{31} in the range 0.1–0.3,

Table 2: Comparison of the elastic moduli for PoSi predicted for a honeycomb structure and obtained from experimental data (the “experimental” value for E_3 is obtained for $\nu_{31} = 0.28$).

Sample	E_3 (GPa)		E'_1 (GPa)	
	pred.	exp.	pred.	exp.
50%	63	12	~ 54	18.6
70%	38	6.5	27	6.2

one finds E_3 to be in the range 20–11 GPa and 11–6 GPa for the 50% and 70% samples.

These small values are compatible with the literature, especially in view of the large dispersion of experimental data. Let us also note that values of E_3 and E'_1 are not very different so that the usual assumption of an isotropic material is *a posteriori* not so bad, at least for porosity in the range 50–70%. The usual interpretation for these small values of Young’s modulus (see, *e.g.*, [14]) is that PoSi is a 3D foam with open cells so that Young’s modulus of bulk Si is reduced by a factor $(1 - p)^2$. However, such a model should not be relevant for our samples and we propose in the following to compare our measurements with the mechanical properties of a honeycomb.

Mechanical properties of a honeycomb are well known [27]. For such a structure, one expects $E_3 = E(1 - p)$ and $\nu_{31} = \nu$, where E and ν are Young’s modulus and Poisson’s ratio of the supposedly isotropic material forming the wall. With $E = 130$ GPa and $\nu = 0.28$, one finds E_3 equals to 63 and 38 GPa for the 50% and 70% samples. Inserting $\nu_{31} = 0.28$ in the above equations yields the experimental values 12 and 6.5 GPa (see table 2 for a summary of expected and measured values). The dependence on porosity is consistent with expectation, but the absolute value of the modulus is roughly 5 times too small. The in-plane properties (ν_{12} and E_1) are structure dependent. For an hexagonal honeycomb, the biaxial modulus $E'_1 = E(t/l)/\sqrt{3}$, where t and l are the thickness and length of the walls perpendicular to the pore axis, respectively. This expression is valid only in the limit of thin walls which is hardly met for our samples (the mean length to thickness ratio, l/t , equals 1.4 and 2.8 for the 50% and 70% samples). Moreover, our samples are random honeycombs so that the expression for E'_1 is only an estimate. One finds that the biaxial modulus E'_1 is about 54 and 27 GPa for the 50% and 70% samples. Again, the experimental values are a few times smaller than the expected ones; for the 70% sample which better satisfies the thin wall limit, the ratio of the experimental value to the expected one is close to 5, similar to the ratio for E_3 .

In sum, all our experimental data are compatible with a honeycomb structure, *provided that Young’s modulus \tilde{E} of the Si walls between pores is 5 times smaller than that of bulk silicon*. This is the first time that such a huge reduction of \tilde{E} is observed, but it is not completely surprising for walls 5–6 nm thick. Indeed, it is well known that finite-size

effects lead to a decrease in the effective Young's modulus [28–30] by a factor which can be as high as 3 for a 12 nm thick cantilever [30]. The size dependence of the effective Young's modulus has been attributed to a number of effects, including surface oxidation, non-linear bulk-elasticity, surface stress effects. . . (see, *e.g.*, [31]). Surface oxidation can be ruled out since we have analyzed our samples a few hours after preparation [32]. Non-linear elasticity is not expected either in view of the low strains we have measured. On the other hand, we must note that the Si walls between pores are rough at an atomic scale and that previous study showed that breaking of Si-Si bonds occurs during the formation of thick PoSi layers [33]. These two points presumably impact the value of \bar{E} but they are not likely to account for the huge reduction in \bar{E} . We think that the surface stress effect is the best candidate to explain this reduction. Clearly, the geometry of the Si walls is not well enough characterized to allow an accurate comparison with the existing models, but our experiments could help to set some limit to model parameters. Our system is also appropriate to study the possible effect of the nature of the liquid surrounding the nano-wall which could impact the surface stress.

Conclusion. – We have performed measurements of anisotropic adsorption-induced strains in porous silicon. The overall shape of the hysteretic strains and adsorption loops are consistent with expectation. In the saturation regime, we measure the elastic responses of the samples to the liquid pressure in the pores. The values of the elastic moduli are consistent with the picture of a honeycomb structure if one assumes that Young's modulus of the silicon wall between the pores is about 5 times smaller than its bulk value. This dramatic reduction could be an extreme case of the well-known finite-size effect observed in nano-wires or nano-cantilevers. Furthermore, the existence of strong surface stress effects supports the idea that thermodynamics of the solid-liquid interface could play an important role in the adsorption phenomenon [6].

REFERENCES

- [1] GROSMA A. and ORTEGA C., *Structural and optical properties of Porous Silicon Nanostructures*, edited by AMATO G., DELERUE C. and VON BARDELEBEN H. J., Vol. **11** (Gordon and Breach Science, London) 1997, p. 317.
- [2] GROSMA A. and ORTEGA C., *Langmuir*, **24** (2008) 3977.
- [3] COASNE B., GROSMA A., ORTEGA C. and SIMON M., *Phys. Rev. Lett.*, **88** (2002) 256102.
- [4] MASON J., *Proc. R. Soc. London, Ser. A*, **390** (1983) 47.
- [5] PUIBASSET J., *J. Chem. Phys.*, **127** (2007) 154701.
- [6] GROSMA A. and ORTEGA C., *Phys. Rev. B*, **78** (2008) 085433.
- [7] DOLINO G., BELLET D. and FAIVRE C., *Phys. Rev. B*, **54** (1996) 17919.
- [8] PRASS J., MÜTER D., FRATZL P. and PARIS O., *Appl. Phys. Lett.*, **95** (2009) 083121.
- [9] BALZER C., WILDHAGE T., BRAXMEIER S., REICHENAUER G. and OLIVIER J. P., *Langmuir*, **27** (2011) 2553.
- [10] SCHAPPERT K. and PELSTER R., *Langmuir*, **30** (2014) 14004.
- [11] GÜNTHER G., PRASS J., PARIS O. and SCHOEN M., *Phys. Rev. Lett.*, **101** (2008) 086104.
- [12] GOR G. Y. and NEIMARK A. V., *Langmuir*, **26** (2010) 13021.
- [13] VANDAMME M., BROCHARD L., LECAMPION B. and COUSSY O., *J. Mech. Phys. Solids*, **58** (2010) 1489.
- [14] BELLET D., LAMAGNÈRE P., VINCENT A. and BRÉCHET Y., *J. Appl. Phys.*, **80** (1996) 3772.
- [15] OISTEN M. and BERGSTROM P., *Phys. Status Solidi A*, **206** (2009) 1278.
- [16] ALIEV G. N., GOLLER B. and SNOW P. A., *J. Appl. Phys.*, **110** (2011) 043534.
- [17] POLOMSKA A. M. and ANDREWS G. T., *Phys. Status Solidi C*, **6** (2009) 1665.
- [18] AMBERG C. H. and MCINTOSH R., *Can. J. Chem.*, **30** (1952) 1012.
- [19] GOR G. Y., PARIS O., PRASS J., RUSSO P. A., RIBEIRO CARROTT M. M. L. and NEIMARK A. V., *Langmuir*, **29** (2013) 8601.
- [20] WATANABE H., ITO N. and HU C. K., *J. Chem. Phys.*, **136** (2012) 204102.
- [21] EPPENGA R. and FRENKEL D., *Mol. Phys.*, **52** (1984) 1303.
- [22] HARISMIADIS V. I., VORHOLZ J. and PANAGIOTOPOULOS A. Z., *J. Chem. Phys.*, **105** (1996) 8469.
- [23] VÖRTLER H. J. and SMITH W. R., *J. Chem. Phys.*, **112** (2000) 5168.
- [24] BARLA K., HERINO R., BOMCHIL G. and PFISTER J. C., *J. Cryst. Growth*, **68** (1984) 727.
- [25] REINHART F. K. and LOGAN A., *J. Appl. Phys.*, **44** (1973) 3171.
- [26] HOPCROFT M. A., NIX W. D. and KENNY T. W., *J. Microelectromech. Syst.*, **19** (2010) 229.
- [27] GIBSON L. J. and ASHBY M. F., *Cellular Solids: Structure and Properties*, edited by CLARKE D. R., SURESH S. and WARD I. M. FRS (Pergamon, New York) 1988.
- [28] ZHU Y., XU Q., FUNG W. Y. and LU W., *Nano Lett.*, **9** (2009) 3934.
- [29] SADEGHIAN H., YANG C. K., GOOSEN J. F. L., VAN DER DRIFT E., BOSSHE A., FRENCH P. J. and VAN DER KEULEN F., *Appl. Phys. Lett.*, **94** (2009) 221903.
- [30] LI X., ONO Y., WANG Y. and ESAHI M., *Appl. Phys. Lett.*, **83** (2003) 3081.
- [31] SADEGHIAN H., VAN DER KEULEN F. and GOOSEN H., *Advances in Micro/Nano Electromechanical Systems and Fabrication Technologies*, edited by TAKAHATA K., Vol. **7** (InTech, City) 2013, p. 155.
- [32] OGATA Y. H., TSUBOI T., SAKKA T. and NAITO S., *J. Porous Mater.*, **7** (2000) 63.
- [33] GROSMA A. and ORTEGA C., *Langmuir*, **25** (2009) 8083.